Science Bulletin 63 (2018) 817–824

Contents lists available at ScienceDirect

Science Bulletin

journal homepage: www.elsevier.com/locate/scib

Science Bulletin
www.scibull.com

Article

A novel superhard tungsten nitride predicted by machine-learning accelerated crystal structure search

Kang Xia [1], Hao Gao [1], Cong Liu, Jianan Yuan, Jian Sun *, Hui-Tian Wang *, Dingyu Xing

National Laboratory of Solid State Microstructures, School of Physics and Collaborative Innovation Center of Advanced Microstructures, Nanjing University, Nanjing 210093, China

ARTICLE INFO

Article history:
Received 2 April 2018
Received in revised form 28 April 2018
Accepted 2 May 2018
Available online 29 May 2018

Keywords:
Tungsten nitride
Transition metal nitrides
Machine-learning accelerated crystal structure searching method
Superhard tungsten nitride

ABSTRACT

Transition metal nitrides have been suggested to have both high hardness and good thermal stability with large potential application value, but so far stable superhard transition metal nitrides have not been synthesized. Here, with our newly developed machine-learning accelerated crystal structure searching method, we designed a superhard tungsten nitride, *h*-WN_6, which can be synthesized at pressure around 65 GPa and quenchable to ambient pressure. This *h*-WN_6 is constructed with single-bonded armchair-like N_6 rings and presents ionic-like features, which can be formulated as $W^{2.4+}N_6^{2.4-}$. It has a band gap of 1.6 eV at 0 GPa and exhibits an abnormal gap broadening behavior under pressure. Excitingly, this *h*-WN_6 is found to be the hardest among transition metal nitrides known so far (Vickers hardness around 57 GPa) and also has a very high melting temperature (around 1,900 K). Additionally, the good gravimetric (3.1 kJ/g) and volumetric (28.0 kJ/cm^3) energy densities make this nitrogen-rich compound a potential high-energy-density material. These predictions support the designing rules and may stimulate future experiments to synthesize superhard and high-energy-density material.

1. Introduction

Transition-metal nitrides (TMNs) are promising candidates for new ultra-hard materials [1–5], due to their outstanding properties, such as comparable thermodynamic stability to cubic γ-Si_3N_4, high melting points, good chemical inertness, high incompressibility and hardness, as well as their better performance in cutting ferrous metals than diamond [6]. It has been found that strong covalent bonding between nitrogen atoms in TMN structures plays a key role in increasing their elastic stiffness and hardness [7]. To synthesize this kind of compounds, high pressure and high temperature (HPHT) conditions are necessary to overcome the energy barriers of breaking nitrogen molecules and mixing elements. For instance, 4*d*- and 5*d*-transition-metal dinitrides with single-bonded N-N pairs were reported to be synthesized with HPHT method, including PtN_2, IrN_2, OsN_2, and PdN_2 [8–12]. Their bulk moduli were measured to be comparable to that of diamond. Recently, the δ-MoN resintered at 5–8 GPa and 1,400–1,800 °C, was reported to be the hardest TMN with superconducting properties, its hardness reaches about 30 GPa [13]. The covalent Mo-N bonded was suggested to enhance the hardness.

Based on first-principles calculations, several superhard TMNs (Vickers hardness >40 GPa) have been proposed. For example, a high nitrogen content *Imm*$_2$-ReN_3 with high hardness of 44.4 GPa, was predicted to be stable under high pressure above 40 GPa [14]. Polyhedral stacking with strong covalent N-N bonds was suggested to remarkably improve the mechanical performance. Another superhard hcp CrN_2 was predicted to be energetically stable at pressures above 7 GPa, possessing a hardness of 46 GPa [15]. The superhardness effect was attributed to the strong electron localization into *p*–*d* orbital hybridization, induced by the N-N interstitial pre-compression. On the other hand, nitrogen-rich compounds have been considered as potential high-energy-density materials [16–21]. Recent theoretical predictions found that nitrogen can form rings at high pressure [19–21].

Among transition-metal nitrides, molybdenum and tungsten nitrides were found to possess the highest hardness and to be comparable to those of *c*-BN [6,22]. Several tungsten nitrides have been successfully synthesized, for instance, rock-salt WN and hexagonal WN (δ-WN) [23], hexagonal and rhombohedral W_2N_3, and cubic W_3N_4 [22]. On the theoretical side, several other W-N compounds with large elastic properties were predicted [24–28]. For instance, the NbO-WN (space group (S.G.) is $Pm\bar{3}m$), NiAs-WN (S.G. is $P\bar{6}m2$) and MoS_2 type W_2N compounds were predicted to possess relatively large bulk (B >300 GPa) and shear (G >200 GPa) moduli [25,27]. A hexagonal $P\bar{6}m2$ of WN_2 was calculated to possess high

* Corresponding authors.
E-mail addresses: jiansun@nju.edu.cn (J. Sun), htwang@nju.edu.cn (H.-T. Wang).
[1] These authors contributed equally to this work.

https://doi.org/10.1016/j.scib.2018.05.027
2095-9273/

hardness of 36.6 GPa [24]. Another W_5N_6 compound was proposed to have hardness of 28 GPa [28], comparable to that of α-SiO_2 [29]. Very recently, the extraordinary strain stiffening in a *hP*6-WN_2 structure was reported to remarkably enhance the indentation strength, which exceeds the threshold of superhard materials (40 GPa) [30].

We can infer from the aforementioned examples that the covalent N-related bonds, especially the N-N single bond, have an important influence on the stiffness and hardness of TMNs. Meanwhile, the isotropy or homogeneity in the direction of covalent bonds largely affects the shear modulus of materials, and thus also influences their hardness. Nice examples for this can be found in ultra-incompressible transition-metal borides (bulk modulus >300 GPa) [31–34]. On the other hand, the metallicity of materials will largely reduce their hardness [35–37]. From the aforementioned observations, three clues seem to be useful for designing hybrid superhard materials containing transition metal and light elements as follows. (1) The candidate should be thermodynamically stable at high pressure and also dynamically stable at ambient pressure, allow us to be able to synthesize it eventually. (2) The good candidate must have a band gap, that is to say, it must be a non-metal. (3) The ratio of light element relative to transition metal atoms must be large enough so that the light element atoms can form strong covalent bonds or even networks and frameworks. These clues inspire us to explore special N-related networks in TMNs, such as rings and even cages, where the short and strongly directional N-N covalent bonds should lead to the super-hardness.

In this work, to perform extensive structure search efficiently, we develop a machine-learning accelerated crystal structure prediction method by combining *ab initio* calculations and Bayesian optimization. Taking W-N binary system as a test for this brand new method, we investigate its phase diagram over a wide pressure range of 0–100 GPa. New ground-state and high-pressure phases at ratios of 1:1 and 1:6 are predicted. Interestingly, the newly found WN_6 is a superhard material containing N_6 rings, its Vickers hardness is evaluated to be around 57 GPa. The novel N_6 rings in WN_6 are found to be essential for the exotic electronic structures and excellent mechanical properties.

2. Materials and methods

2.1. Machine-learning accelerated crystal structure searching

Recently, many methods have been developed to search or predict crystal structures at ambient or extreme conditions [38–47]. The common goal of these methods is to find the global and/or local minima of the free energy surface. Many theoretical predictions have been verified by experiments, which validate these methods. However, the crystal structure searching process based on *ab initio* calculations are expensive, and the most time-consuming part is the total energy calculations for each crystal structure. How to raise the efficiency (to accelerate predictions) is a significant challenge. Here we proposed and implemented a machine-learning accelerated crystal structure prediction method based on Bayesian optimization [48] to improve the search efficiency and diversity. The complete algorithm process is depicted in the left panel of Fig. 1. Mutation and heredity operators are used to generate new structures within an evolutionary fashion. The energies for the structures can be predicted by a Gaussian Process model, which is one of the major branches of the machine-learning algorithm [49,50]. An acquisition function, $F(x) = \mu(x) + k\sigma(x)$, is used to select the structures for the next generation, where $\mu(x)$ and $\sigma(x)$ represent the mean and standard deviations of the predictive distribution at the x point in the structural space, respectively. The maxima of this function are the points with both higher uncertainties and better prediction values, which is a trade-off between the exploration (wide range exploration on the energy surface) and exploitation (careful search near the local minima of the energy surface), as one can see from the right panel of Fig. 1. More details about the method can be found in the Supplementary data.

2.2. Computational codes

We used the VASP code [51] to perform the structure optimizations and enthalpy calculations. The Perdew-Burke-Ernzerh functional was applied within the generalized gradient approximation (GGA-PBE) [52]. The projector-augmented wave (PAW) method was adopted [53]. The structures were relaxed at a high level of accuracy, consisting of a kinetic energy cutoff of 1,050 eV, using a k-mesh of spacing $2\pi \times 0.03$ Å^{-1} in the Brillouin Zone. Electronic localization functions (ELF) calculated by VASP were displayed by the Visualization for Electronic and STructural Analysis (VESTA) [54]. Electronic band structures and partial densities of states were computed by the WIEN2k code [55]. The hybrid Heyd-Scuseria-Ernzerhof functional (HSE06) [56,57] was also used to achieve accurate electronic band structures. Phonon modes and frequencies of the stable structures were calculated by the PHONOPY code [58], combined with the VASP code. Elastic properties were computed by VASP, and the bulk and shear modulus were calculated based on Voigt averaging [59]. And the Vickers hardness was computed by model of Chen et al. [60] and Tian et al. [36]. The melting point and thermal stability of *h*-WN_6 are studied by *ab initio* molecular dynamics (AIMD) simulations in the *NVE* [61] and *NpT* ensembles [62] respectively. All MD simulations are performed for the $\sqrt{2} \times 2\sqrt{2} \times 3$ supercell of WN_6 conventional cell, containing 252 atoms. The data points in *Z*-method [61] calculations dotted in two *Z* curves, are obtained by statistics over the last 2 ps in every trajectory. The simulation runs to 36 ps with a time step of 1 fs using the *NpT* ensemble with a Langevin thermostat.

3. Results

3.1. The enthalpical stability

Using our machine-learning accelerated first-principles crystal structure prediction method (Fig. 1), a series of convex hulls are obtained at pressures of 0, 20, 50 and 100 GPa (Fig. S1 online). Two new W-N compounds at ratios of 1:1 and 1:6 (W:N) are found. The pressure-concentration diagram of stable W-N compounds is plotted in Fig. 2a. The newly predicted WN_6 (S.G. $R\bar{3}m$; we named as *h*-WN_6), is labeled by blue and italic font (Fig. S1 online). It emerges at pressure of 100 GPa and is enthalpically favorable over a pressure range of 65–100 GPa (Fig. 2a). The enthalpy of another new W-N phase (S.G. $P\bar{6}m2$) with 1:1 ratio (we named as *h*-WN) is very close to that of the NiAs-WN structure [25] in the pressure range of 20–45 GPa.

The formation enthalpy of N-rich *h*-WN_6 becomes negative at high pressures >31 GPa (Fig. 2b), which indicates its possible formation from elemental tungsten and nitrogen phases. Therefore, high-pressure synthesis of *h*-WN_6 can be achieved in the reactions of WN + 5N → WN_6 (green solid line) and WN_2 + 4N → WN_6 (blue dotted dash line), at high pressures >50 and 65 GPa respectively (Fig. 2d). Here "N" represents one nitrogen atom in the typical stable structures of nitrogen under different pressures, such as the $P4_12_12$ N_2 molecular structure (<60 GPa) and the cg-N polynitrogen (>60 GPa). The formation enthalpy of $P\bar{6}m2$ WN is found to be negative and decrease monotonically with increasing pressure (Fig. 2b). At zero temperature, $P\bar{6}m2$ phase WN predicted in this work becomes more favorable than the NbO-WN structure [27] at pressure of 20 GPa (Fig. 2c). With further increasing the pressure

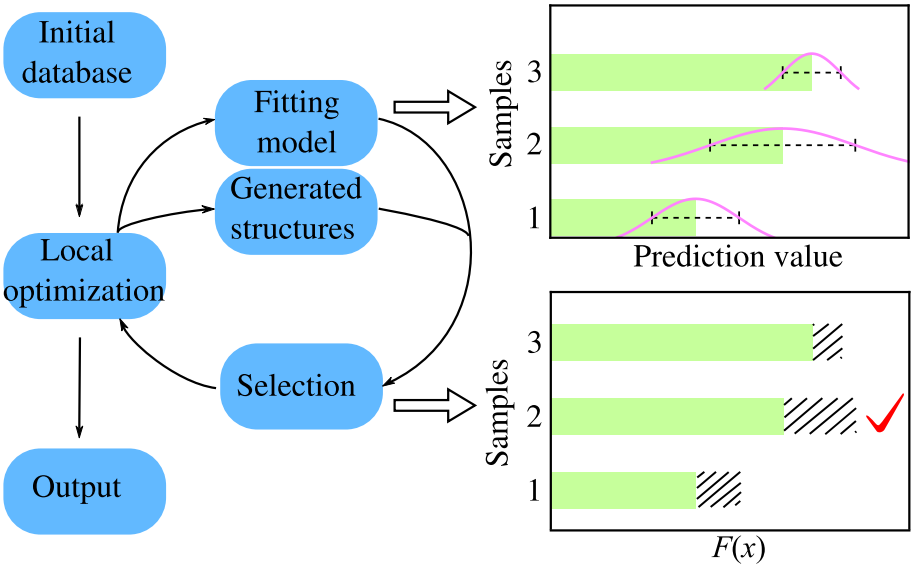

Fig. 1. (Color online) Flow chart of the machine-learning accelerated crystal structure prediction method. Bayesian optimization, and the strategies of model fitting and selection are shown in the left, and the right panel, respectively. In the upper part of right panel, the Gaussian distributions and uncertainties are depicted by pink solid curves and black dashed lines, respectively. The lower part shows the selection process by comparing the acquisition function based on the model. The estimated uncertainties are filled by black twills and the total bars represent the values of the acquisition function $F(x)$. Here the second sample is regarded as the best prediction choice (red tick) for its highest value of $F(x)$ ($k = 1$), although the predicted average value is lower than the third sample.

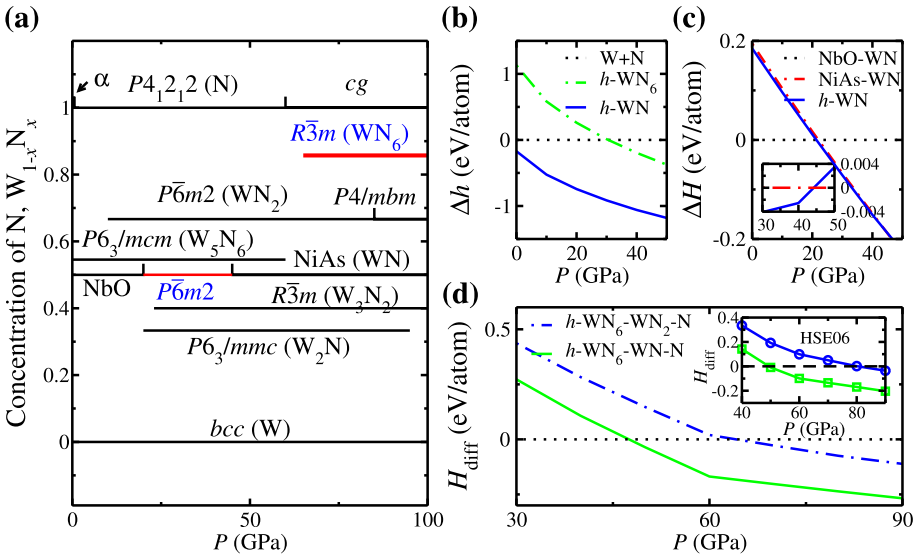

Fig. 2. (Color online) The theoretical energy-pressure relationships of W–N system. (a) The corresponding pressure-concentration diagram of stable phases. Here black ones are previously known W-N compounds. (b) The formation energy versus pressure relations of $R\bar{3}m$ WN_6 (h-WN_6) and $P\bar{6}m2$ WN (h-WN) predicted in this work. (c) and (d) The enthalpical differences versus pressure relations of $P\bar{6}m2$ WN and $R\bar{3}m$ WN_6, respectively. Black dotted line in (d) represents the mixture of WN and N or WN_2 and N. Inset of (d) shows the enthalpy-pressure curves from HSE06 calculations. Blue circle-solid line is the enthalpy difference for the reaction of $WN_2 + 4N \rightarrow WN_6$, and the green square-solid line is for the $WN + 5N \rightarrow WN_6$ reaction.

up to 45 GPa, WN transforms from the $P\bar{6}m2$ phase to NiAs-WN structure [25]. The enthalpy of $P\bar{6}m2$ WN structure is slightly lower than that of NiAs-WN at pressures of 20–45 GPa (about 4 meV/atom at 30 GPa as shown in the inset of Fig. 2c), which makes them more or less overlap with each other in the convex-hull diagram. Thus the $P\bar{6}m2$ WN structure predicted in this work fills in a gap in the pressure range of 20–45 GPa in the previous reported phase diagram of WN [28].

The hybrid HSE06 functionals sometimes provide more accurate description of energetics than GGA, such as in crystalline carbon, bromine and iodine, where the GGA-PBE method fails [63,64]. To verify our PBE enthalpy results, we have optimized the stable W-N structures ($P4_12_12$ N_2, cg-N, NiAs-WN, $P\bar{6}m2$ WN_2, $P4/mbm$ WN_2, and $R\bar{3}m$ WN_6) using the hybrid HSE06 functionals at six pressure points in the range of 40–90 GPa. The enthalpy differences are exhibited in the inset of Fig. 2d. Compared to PBE results in Fig. 2d, we find the transformation pressure for the reaction $WN_2 + 4N \rightarrow WN_6$ (blue circle-solid line) just shift to about 80 GPa. The transition pressure of the other reaction $WN + 5N \rightarrow WN_6$ (green square-solid line) stays almost the same. These HSE06 data shows that our GGA-PBE results are valid in the W-N system.

3.2. The crystal and electronic structure

The crystal structures of $P\bar{6}m2$ WN and $R\bar{3}m$ WN_6 are shown in Fig. 3c and a, b, respectively. Their structure details are listed in Table S1 (online). The $P\bar{6}m2$ WN can be constructed from the NiAs-WN conventional cells [25] with *AB* stacking along the [001] direction. Interestingly, the $R\bar{3}m$ WN_6 is composed of tungsten atoms and armchair-like N_6 (*ac*-N_6) rings (Fig. 3a and b). Viewed from the [100] direction, the WN_6 phase also looks like a sandwich structure. The bond distance between tungsten atom and its nearest neighboring nitrogen atoms (d_{W_N}) is about 2.27 Å. The distance between the N atoms (d_{N_N}) in the N_6 ring is around 1.43 Å at 0 GPa, which is close to the bond length of N_2 pair in PtN_2 [9]. This bond length is nearly identical to that the N-N bond in the hydrazine molecule (1.45 Å) at ambient pressure. Thus the N-N single bonds form the N_6 ring. The strong covalent bonding N_2 pair in PtN_2 has been found to be beneficial to stabilize the crystal structure and enhance the high elastic moduli of PtN_2 [65]. This inspires us to study the bonding nature of *ac*-N_6 in *h*-WN_6.

We have calculated the electron localization function (ELF) of *h*-WN_6 for bonding analysis. The contour plot of three-dimension ELF is projected in the (001) plane and cutting through the center of a N_6 ring (Fig. 3d). Valence electrons of W and N atoms are obviously found to localize along W-N and N-N bonding directions. ELF contour cutting through three neighboring N atoms (yellow marks) in a N_6 ring and along the (110) plane are presented in Fig. 3e and f, respectively. The high localization for the N-N bonds and the lone pairs on the nitrogen atoms can be seen clearly. To quantify the charge transfer between W and N atoms in the WN_6 cells, Bader's theory of atoms-in-molecules is employed [66]. The Bader charge analysis reveals that the total charge from one W atom to one N_6 ring is around 2.4*e*. This indicates that the *h*-WN_6 phase predicted here possesses some kind of ionic-like feature. This type of charge transfer and ionic-like feature in noble metal nitrides has been suggested to be one of the major sources of their huge bulk moduli [67]. Actually an isostructural stable XeN_6 with similar ionic feature has been predicted under high pressures [68].

To discuss the dynamical stability of the WN_6 phase, phonon dispersions are calculated at 0 GPa (Fig. 4a), where there is no any imaginary frequency found. This suggests that this high-pressure $R\bar{3}m$ phase is metastable and can be recovered to ambient pressure, which may be useful in real applications. Additionally, the energetically stable $P\bar{6}m2$ WN, is also dynamically stable judged from phonon spectra (Fig. S2a online).

This *h*-WN_6 is estimated to be a semiconductor with small indirect band gap (E_g) by the electronic structures calculation (the left panel of Fig. 3g). E_g is evaluated to be around 0.9 eV at 0 GPa, which changes very little with spin-orbit coupling (Fig. S3 online). The valence band maximum and conduction band minimum are located at *Z* and *L* in the first Brillouin Zone, respectively. Results of partial DOS (the right panel of Fig. 3g) reveal that W-5*d* and N-2*p* orbits make main contributions to the conduction bands in the energy interval of 1.0–4.0 eV and to the valence bands of −3.0 to 0 eV, respectively. The indirect band gap is closely related

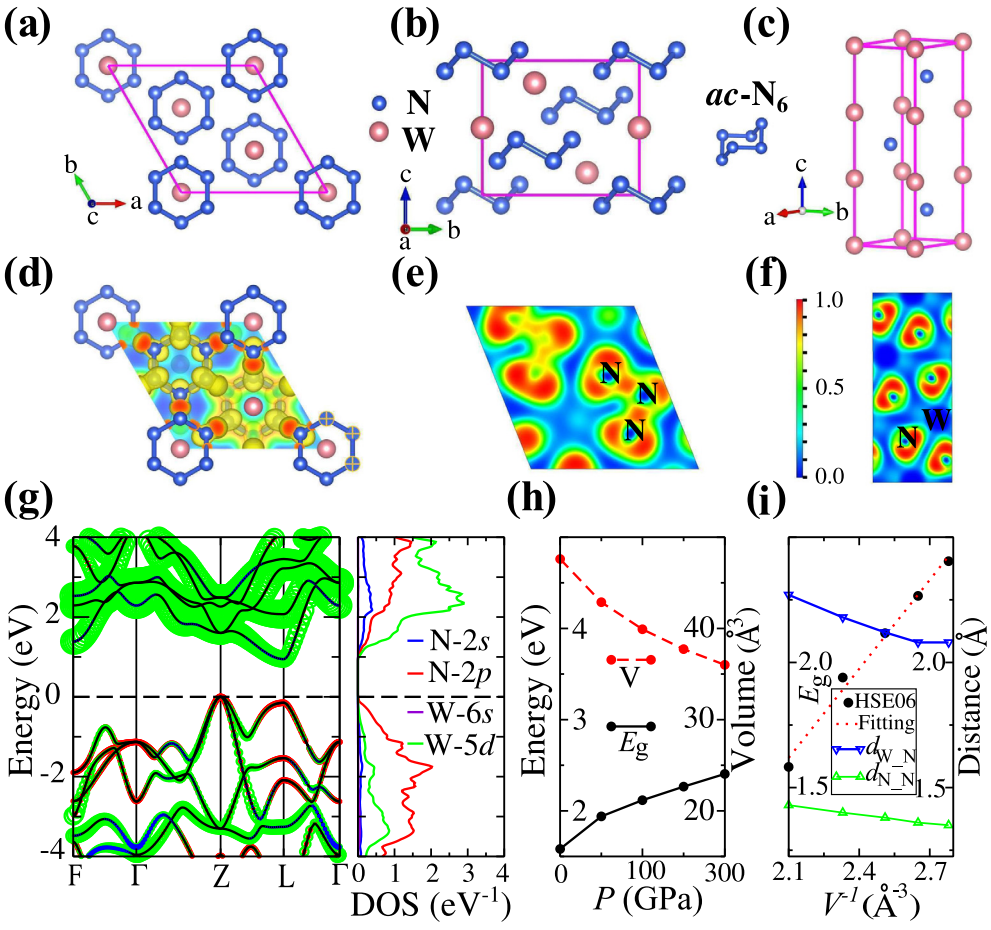

Fig. 3. (Color online) Crystal structrure and theoretical electronic structures of new W–N phases. (a)–(c) Crystal structures for *h*-WN_6 and *h*-WN. (d)–(f) The electron localization functions (ELF) contour plot of *h*-WN_6. (g) Electronic band structures (left panel) and partial DOS (right panel) of *h*-WN_6 at 0 GPa. (h) HSE06 results of band gap (E_g) and equilibrium volume (*V*) versus pressure. (i) E_g, d_{W_N} and d_{N_N} versus corresponding V^{-1}. The ELF contour maps of *h*-WN_6 are plotted in (d) with an isosurface value of 0.8 *e*/Bohr^3. Colored lines in (g) characterize the main contributions from atomic orbitals to bands. The zero energy is set to the top of the valence band.

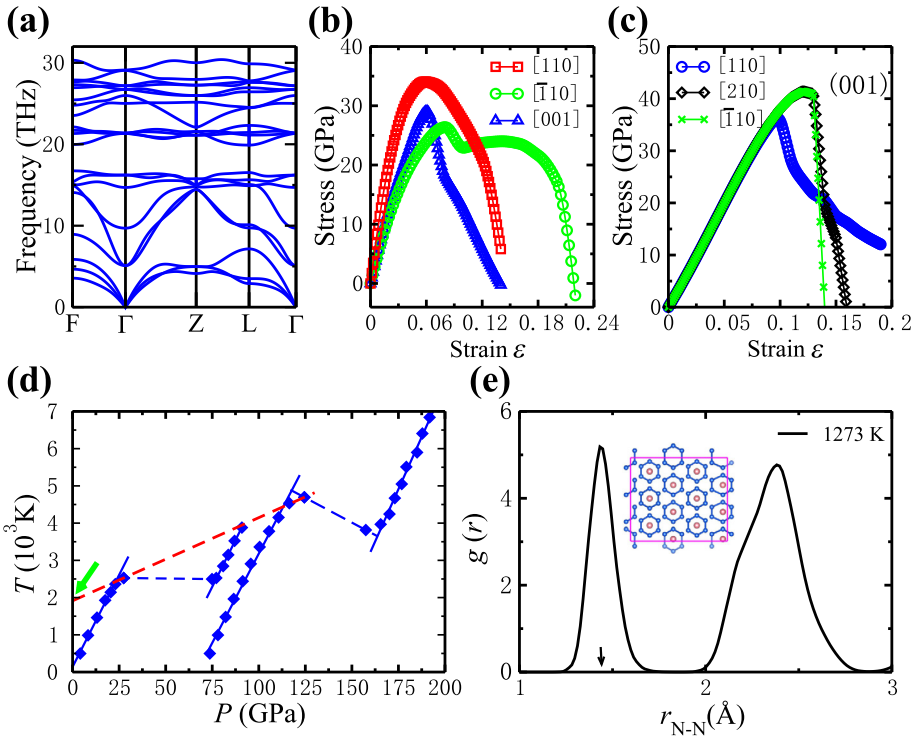

Fig. 4. (Color online) Theoretical phonon, strain-stress relation, melting point and thermal stability calculations of *h*-WN_6. (a) Phonon dispersion curves of WN_6 at 0 GPa. (b) Calculated stresses under the ideal tensile strains along the [$\bar{1}$10], [110], and [001] directions. (c) Calculated stress responses to the Vickers indentation shear strains in the (001) plane along the [$\bar{1}$10], [110] or [210] shear direction. (d) Melting temperature at ambient pressure (green arrow) estimated using *Z* method for *h*-WN_6. (e) Pair distribution functions $g(r)$ for the N-N pairs observed during AIMD simulations for *h*-WN_6 at ambient pressure and temperature of 1,273 K. The red dashed line in (d) represents the estimated melting curve. Inset in (e) is the statistically average structure at temperature of 1,273 K. The black arrow represents the average closest N-N distance in the *ac*-N_6 ring.

to W-5*d* occupied and N-2*p* bonding states. The W-6*s* electrons almost have no contribution to the DOS around the Fermi level, which also indicates that they may transfer into localized states, as we see from the charge analysis.

The energy gap of WN_6 under ambient pressure is evaluated to be 1.58 eV from the hybrid HSE06 functional, which is around 0.68 eV larger than that calculated by PBE functional. This gap monotonously increases to 2.40 eV with increasing pressure to 200 GPa (Fig. 3h), which behaves in the opposite way, compared with that of usual semiconductors, where the band gap usually becomes narrow upon compression. To get a clear understanding of this odd band-gap behavior of *h*-WN_6, we further study the responses of equilibrium volume (V) and atomic distances to external pressures, as depicted in Fig. 3h and i, respectively. Our calculations show that E_g of WN_6 has a linearly dependence on $1/V$ (Fig. 3i). And d_{W_N} decreases more quickly than d_{N_N} with compressed volume, which means that the N-N bonds in the N_6 rings are very strong compared to the W-N interactions. With the formation of the N_6 ring, there are still three valence electrons left for one nitrogen atom. Therefore, some electrons transfer from tungsten atom to nitrogen atom, forming two lone pairs. There is rather strong repulsion between the lone pairs, and between them and other electronic states, which opens a gap in this compound. With compression, the repulsions get even stronger when the volume gets smaller, making the energy gap even bigger. Moreover, we calculated the band structure and the partial DOS of WN_6 under pressure of 100 GPa (Fig. S4 online). The band structure keeps almost the same to that under 0 GPa. While the W and N atoms in the high-pressure structure make much less orbital contribution to the DOS, compared with that under 0 GPa, especially for the W 5*d* orbital electrons around the energy level of the conduction band minimum. This seems to have come from the strong repulsion between electron lone pairs and other valence electrons, resulting in much lower occupation in the high-energy-level W-N bonded states than that in the low-energy-level N-N single bonded states under compression.

3.3. The superhardness, thermal stability and high energy density

We further study the elastic properties of *h*-WN_6 and *h*-WN. The calculated elastic constants are listed in Table 1, compared with the experimental results of *δ*-MoN [13]. The calculated bulk modulus B and shear modulus G of *h*-WN_6 are 302.7 and 315.7 GPa respectively. Although its bulk modulus is not the highest in transition metal nitride, the high values of both G and Pugh modulus ratio (G/B >1.0) indicate that the *h*-WN_6 may have high Vickers hardness. The hardness value of WN_6 is estimated by semi-empirical models and exact strain-stress calculations. Using the methods of Chen et al. [60] and Tian et al. [36], the Vickers hardness of WN_6 is estimated to be about 57.9 and 56.8 GPa, respectively, which is much harder than the previously known hardest experimental synthesized transition metal nitride *δ*-MoN (H_v = 30 GPa) [13] and also the theoretically predicted *hP*6-WN_2 (H_v = 46.7 GPa) [30]. Therefore, *h*-WN_6 is a potential superhard material, hitting the highest record in the Vickers hardness of transition metal nitride up to now. To cross check the stress-strain responses to the atomic deformation similar to the process in the experimental nano indentation hardness test, we calculate the Vickers indentation shear strength (the centerline-to-face angle equals 68 °) of *h*-WN_6 with the method from Refs. [69] and [30]. As shown in Fig. 4b, its peak stress under ideal tensile strains along the [001] direction is found to be weaker than that along the [$\bar{1}$10] and [110] directions. Thus we evaluate the stresses in the easy cleavage plane of (001), under the Vickers indentation shear strains along three high-symmetry directions [$\bar{1}$10], [110] and [210]. As shown in Fig. 4c, using GGA-PBE method we obtain a

Table 1
Mechanical properties of several W/Mo–N compounds. Here list the calculated elastic constants C_{ij} (GPa), bulk and shear moduli (B and G) (GPa), and the Vickers' hardness of our $R\bar{3}m$ h-WN_6, $P\bar{6}m2$ h-WN and h-MoN_6 by PBE calculations at 0 GPa, in comparison with hexagonal WN_2 and δ-MoN. H_v, H_{vc} and H_{vt} represent the Vickers hardness from the experiments, estimated from the methods of Chen et al. [60], and Tian et al. [36], respectively.

Compounds	Work	C11	C12	C13	C33	C44	C66	B	G	H_{vc}	H_{vt}	H_v
δ-MoN	This work	570.3	213.9	243.8	768.5	282.9	178.2	368.0	229.3	24.6	25.2	–
	Experiment [13]	–	–	–	–	–	–	335	220	–	–	30
h-WN_6	This work	662.1	76.1	132.9	716.5	359.6	293.0	302.7	315.7	57.9	56.8	–
h-WN	This work	685.9	208.9	247.3	721.6	239.0	238.5	388.9	236.0	24.2	24.9	–
h-MoN_6	This work	551.4	68.2	114.1	625.0	312.2	241.6	257.9	268.6	52.3	50.6	–

lowest Vickers indentation shear strength of around 37.3 GPa at a peak-stress strain of 0.10 for the (0 0 1) plane shearing in the [1 1 0] direction. The pure shear strength [70] shown in Fig. S5a (online) is slightly smaller than the Vickers indentation shear strength, which is similar to cases in other systems [69,30]. However, the Vickers indentation shear strength usually has a much better agreement with the experimentally measured Vickers hardness than the pure shear strength [69,30]. Moreover, the Vickers indentation strain-stress calculations by LDA method can give more accurate Vickers hardness estimation comparable to the experimental values. For example, the Vickers indentation strengths of diamond and c-BN based on LDA calculations, are estimated to be around 96.6 and 60.4 GPa (right panels of Fig. S5c and S5d online) respectively, which are closer to the experimental values (diamond ~100 GPa, c-BN ~55 GPa) than GGA-PBE results (diamond ~94.1 GPa, c-BN ~63.5 GPa) (left panels of Fig. S5c and S5d online) [69]. LDA calculations for the Vickers indentation deformations of WN_6 estimate a shear strength of 48.6 GPa at a peak-stress strain of 0.12 for the (0 0 1) [1 1 0] shearing direction (Fig. S5b online), which is consistent with the model results (H_{vc} ~57.9 GPa, H_{vt} ~56.8 GPa) in Table 1.

TMNs are widely studied as hard materials not only because of their outstanding mechanical property, but also for their thermal stability and high melting points [6]. We estimated the melting point of superhard h-WN_6 by employing the Z method [61] (Fig. 4d). The melting temperature is evaluated to be ~1,900 K, by the coexistence of solid and liquid phase in two Z curves. Thus the melting temperature of h-WN_6 structure is considerably higher compared to other nitrides [6]. We also cross check its thermal stability by performing *ab initio* molecular dynamics (AIMD) simulations (Figs. 4 and S6). During the entire AIMD simulations running for more than 36 picoseconds using NpT ensemble [62] at temperature of around 1,273 K, the h-WN_6 structure stays intact and the covalent N-N bonds in ac-N_6 rings are not broken. The statistically averaged closest N-N bond length is around 1.44 Å (Fig. 4e). These simulations suggest that the N_6 rings are kinetically quite stable and can be successfully preserved at ambient pressure and high temperatures. The AIMD parameters we choose are reasonable after convergence tests (Fig. S7 online).

Since hexagonal δ-MoN was proposed to be very hard [2,13], we replace the W atom of h-WN_6 with Mo atom, and find out the synthesis of an isomorphic h-MoN_6 is also possible at around 95 GPa (Figs. S2b and S8). The Vickers hardness of h-MoN_6 is calculated to be 50.6 GPa, as listed in Table 1, which indicates that h-MoN_6 is another superhard material candidate.

Moreover, we calculated that h-WN_6 can release about 8.73 eV/f.u. chemical energy during the reaction of $5WN_6 \rightarrow W_5N_6 + 12N_2$ at 0 K and 0 GPa, which is higher than that of $Immm$-HfN_{10} per formula [18]. The gravimetric energy density for h-WN_6 is estimated to be around 3.1 kJ/g. the unique N_6 ring in h-WN_6 results in a volume (V) reduction of 50% per formula (f.u.) ($V \sim 49.84$ Å^3/f.u.) to that of high-density-energy HfN_{10} (104.3 Å^3/f.u.) under ambient pressure. Much volumeric reduction for h-WN_6 leads to the dense volumetric energy density estimated to be around 28.0 kJ/cm^3, which is much higher than those of MN_{10} (M = Hf, Zr, and Ti) and is almost four times as much as that of TNT (7.2–8.0 kJ/cm^3).

4. Conclusion

In summary, we developed a new machine-learning accelerated methodology for crystal structure searching based on Bayesian Optimization and *ab initio* calculations. Three guiding factors seem to be important for designing hybrid superhard compounds with transition metal and light elements: the structural stability, the non-metallicity, and a large ratio of light elements. As a test case for both our method and these guiding rules, a systematic search for the stable phases in W-N system has been performed over a pressure range of 0–100 GPa. Two new tungsten nitrides ($P\bar{6}m2$ WN and $R\bar{3}m$ WN_6) are predicted to be stable under high pressures and metastable at ambient conditions. Interestingly, the $R\bar{3}m$ WN_6 contains armchair-like N_6 rings with pure N-N single bonds. There is considerable charge transfer between the tungsten atoms and the N_6 rings in this compound, making it exhibit some ionic features. Different from the usual semiconductors, the band gap of this compound has an abnormal broadening behavior under pressure, which mainly due to the repulsion between the lone pairs in the N_6 rings. Even more excitingly, h-WN_6 is estimated to possess the Vickers hardness of 57 GPa by microscopic hardness models. This value sets the highest hardness record of transition metal nitrides. Its superhardness is cross checked by Vickers indentation shear stiffening calculations. This superhard WN_6 structure also has very good thermal stability with a high melting point of ~1,900 K. The good gravimetric (3.1 kJ/g) and volumetric (28.0 kJ/cm^3) energy densities make this nitrogen-rich compound a potential high-energy-density material. During the long review process of this work on different journals, we recently noticed that another work [71] also predicted the same WN_6 structure, however these two pieces of work are completely independent. We believe these predictions will stimulate future experiments to synthesize this superhard and high-energy-density material with interesting electronic properties.

Conflict of interest

The authors declare that they have no conflict of interest.

Acknowledgments

This work was financially supported by the Ministry of Science and Technology of the People's Republic of China (2016YFA0300404 and 2015CB921202), the National Natural Science Foundation of China (51372112 and 11574133), the NSF of Jiangsu Province (BK20150012), the Fundamental Research Funds for the Central Universities, the Science Challenge Project (TZ2016001) and Special Program for Applied Research on Super Computation of the NSFC-Guangdong Joint Fund (the second phase) under Grant No. U1501501. Some of the calculations were performed on the supercomputer in the High Performance Computing Center of Nanjing University and "Tianhe-2" at NSCC-Guangzhou.

Author contributions

J. S. designed and supervised the project. K. X. designed the structure, performed *ab initio* calculations; H. G. and J. S. developed the new machine-learning accelerated crystal structure searching method; C. L. analyzed the bond lengths and structure in AIMD simulations, performed *Z*-method calculations; Jianan Yuan helped to check the stress-strain calculations; K. X., J. S., H. T. W. and D. Y. X. wrote the paper. All authors discussed the results and commented on the manuscript.

Appendix A. Supplementary data

Supplementary data associated with this article can be found, in the online version, at https://doi.org/10.1016/j.scib.2018.05.027.

References

[1] Haines J, Leger JM, Bocquillon G. Synthesis and design of superhard materials. Annu Rev Mater Res 2001;31:1–23.
[2] McMillan PF. New materials from high-pressure experiments. Nat Mater 2002;1:19–25.
[3] Kaner RB, Gilman JJ, Tolbert SH. Materials science – designing superhard materials. Science 2005;308:1268–9.
[4] Solozhenko VL, Gregoryanz E. Synthesis of superhard materials. Mater Today 2005;8:44–51.
[5] Rivadulla F, Banobre-Lopez M, Quintela CX, et al. Reduction of the bulk modulus at high pressure in CrN. Nat Mater 2009;8:947–51.
[6] Friedrich A, Winkler B, Juarez-Arellano EA, et al. Synthesis of binary transition metal nitrides, carbides and borides from the elements in the laser-heated diamond anvil cell and their structure-property relations. Materials 2011;4:1648–92.
[7] Zhao Z, Xu B, Tian Y. Recent advances in superhard materials. Annu Rev Mater Res 2016;46:383–406.
[8] Gregoryanz E, Sanloup C, Somayazulu M, et al. Synthesis and characterization of a binary noble metal nitride. Nat Mater 2004;3:294–7.
[9] Crowhurst JC, Goncharov AF, Sadigh B, et al. Synthesis and characterization of the nitrides of platinum and iridium. Science 2006;311:1275–8.
[10] Young AF, Sanloup C, Gregoranz E, et al. Synthesis of novel transition metal nitrides IrN_2 and OsN_2. Phys Rev Lett 2006;96:155501.
[11] Montoya JA, Hernandez AD, Sanloup C, et al. OsN_2: crystal structure and electronic properties. Appl Phys Lett 2007;90:011909.
[12] Crowhurst JC, Goncharov AF, Sadigh B, et al. Synthesis and characterization of nitrides of iridium and palladium. J Mater Res 2008;23:1–5.
[13] Wang S, Antonio D, Yu X, et al. The hardest superconducting metal nitride. Sci Rep 2015;5:13733.
[14] Zhao Z, Bao K, Li D, et al. Nitrogen concentration driving the hardness of rhenium nitrides. Sci Rep 2014;4:4797.
[15] Zhao Z, Bao K, Tian F, et al. Potentially superhard hcp CrN_2 compound studied at high pressure. Phys Rev B 2016;93:214104.
[16] Mailhiot C, Yang LH, McMahan AK. Polymeric nitrogen. Phys Rev B 1992;46:14419.
[17] Eremets MI, Gavriliuk AG, Trojan IA, et al. Single-bonded cubic form of nitrogen. Nat Mater 2004;3:558–63.
[18] Zhang J, Oganov AR, Li X, et al. Pressure-stabilized hafnium nitrides and their properties. Phys Rev B 2017;95:020103.
[19] Steele BA, Oleynik II. Ternary inorganic compounds containing carbon, nitrogen, and oxygen at high pressures. Inorg Chem 2017;56:13321–8.
[20] Steele BA, Oleynik II. Pentazole and ammonium pentazolate: crystalline hydro-nitrogens at high pressure. J Phys Chem A 2017;121:1809–14.
[21] Steele BA, Oleynik II. Novel potassium polynitrides at high pressures. J Phys Chem A 2017;121:8955–61.
[22] Wang S, Yu X, Lin Z, et al. Synthesis, crystal structure, and elastic properties of novel tungsten nitrides. Chem Mater 2012;24:3023–8.
[23] Wriedt HA. The N-W (nitrogen-tungsten) system. Bull Alloy Phase Diag 1989;10:358–67.
[24] Wang H, Li Q, Li Y, et al. Ultra-incompressible phases of tungsten dinitride predicted from first principles. Phys Rev B 2009;79:132109.
[25] Qin J, Zhang X, Xue Y, et al. Structure and mechanical properties of tungsten mononitride under high pressure from first-principles calculations. Comp Mater Sci 2013;79:456–62.
[26] Yan H, Zhang M, Wei Q, et al. Theoretical study on tetragonal transition metal dinitrides from first principles calculations. J Alloys Compd 2013;581:508–14.
[27] Mehl MJ, Finkenstadt D, Dane C, et al. Finding the stable structures of $N_{1-x}W_x$ with an ab initio high-throughput approach. Phys Rev B 2015;91:184110.
[28] Zhao Z, Bao K, Duan D, et al. The low coordination number of nitrogen in hard tungsten nitrides: a first-principles study. Phys Chem Chem Phys 2015;17:13397–402.
[29] Gao F, He J, Wu E, et al. Hardness of covalent crystals. Phys Rev Lett 2003;91:015502.
[30] Lu C, Li Q, Ma Y, et al. Extraordinary indentation strain stiffening produces superhard tungsten nitrides. Phys Rev Lett 2017;119:115503.
[31] Levine JB, Tolbert SH, Kaner RB. Advancements in the search for superhard ultra-incompressible metal borides. Adv Funct Mater 2009;19:3519–33.
[32] Zang C, Sun H, Tse JS, et al. Indentation strength of ultraincompressible rhenium boride, carbide, and nitride from first-principles calculations. Phys Rev B 2012;86:014108.
[33] Li B, Sun H, Zang C, et al. Fundamental constraints on the strength of transition-metal borides: the case of CrB_4. Phys Rev B 2013;87:174106.
[34] Yeung MT, Mohammadi R, Kaner RB. Ultraincompressible, superhard materials. Annu Rev Mater Res 2016;46:465–85.
[35] Guo X, Li L, Liu Z, et al. Hardness of covalent compounds: roles of metallic component and d valence electrons. J Appl Phys 2008;104:023503.
[36] Tian Y, Xu B, Zhao Z. Microscopic theory of hardness and design of novel superhard crystals. Int J Refract Met Hard Mater 2012;33:93–106.
[37] Wang Q, He J, Hu W, et al. Is orthorhombic iron tetraboride superhard? J Materiomics 2015;1:45–51.
[38] Laio A, Parrinello M. Escaping free-energy minima. Proc Natl Acad Sci USA 2012;99:12562–6.
[39] Goedecker S. Minima hopping: an efficient search method for the global minimum of the potential energy surface of complex molecular systems. J Chem Phys 2004;120:9911–7.
[40] Glass CW, Oganov AR, Hansen N. USPEX – evolutionary crystal structure prediction. Comput Phys Commun 2006;175:713–20.
[41] Yao Y, Tse JS, Tanaka K. Metastable high-pressure single-bonded phases of nitrogen predicted via genetic algorithm. Phys Rev B 2008;77:052103.
[42] Wang Y, Lv J, Zhu L, et al. Crystal structure prediction via particle-swarm optimization. Phys Rev B 2010;82:094116.
[43] Pickard CJ, Needs RJ. Ab initio random structure searching. J Phys Condens Matter 2011;23:053201.
[44] Lonie DC, Zurek E. XTALOPT: an open-source evolutionary algorithm for crystal structure prediction. Comput Phys Commun 2011;182:372–87.
[45] Tipton WW, Hennig RG. A grand canonical genetic algorithm for the prediction of multi-component phase diagrams and testing of empirical potentials. J Phys Condens Matter 2013;25:495401.
[46] Wu S, Ji M, Wang C, et al. An adaptive genetic algorithm for crystal structure prediction. J Phys Condens Matter 2014;26:035402.
[47] Zhang Y, Gao W, Chen S, et al. Inverse design of materials by multi-objective differential evolution. Comp Mater Sci 2015;98:51–5.
[48] Shahriari B, Swersky K, Wang Z, et al. Taking the human out of the loop: a review of bayesian optimization. Proc IEEE 2016;104:148–75.
[49] Behler J, Parrinello M. Generalized neural-network representation of high-dimensional potential-energy surfaces. Phys Rev Lett 2007;98:146401.
[50] Bartók AP, Payne MC, Kondor R, et al. Gaussian approximation potentials: the accuracy of quantum mechanics, without the electrons. Phys Rev Lett 2010;104:136403.
[51] Kresse G, Furthmuller J. Efficient iterative schemes for ab initio total-energy calculations using a plane-wave basis set. Phys Rev B 1996;54:11169–86.
[52] Perdew JP, Burke K, Ernzerhof M. Generalized gradient approximation made simple. Phys Rev Lett 1996;77:3865–8.
[53] Blochl PE. Projector augmented-wave method. Phys Rev B 1994;50:17953.
[54] Momma K, Izumi F. VESTA 3 for three-dimensional visualization of crystal, volumetric and morphology data. J Appl Crystallogr 2011;44:1272.
[55] Blaha P, Schwarz K, Sorantin P. Full-potential, linearized augmented plane-wave programs for crystalline systems. Comput Phys Commun 1990;59:399–415.
[56] Heyd J, Scuseria GE, Ernzerhof M. Hybrid functionals based on a screened coulomb potential. J Comp Phys 2006;124:219906.
[57] Paier J, Marsman M, Hummer K, et al. Screened hybrid density functionals applied to solids. J Comp Phys 2006;124:154709.
[58] Togo A, Tanaka I. First principles phonon calculations in materials science. Scr Mater 2015;108:1–5.
[59] Hill R. The elastic behaviour of a crystalline aggregate. Proc Phys Soc Sect A 1952;65:349.
[60] Chen X, Niu H, Li D, et al. Modeling hardness of polycrystalline materials and bulk metallic glasses. Intermetallics 2011;19:1275–81.
[61] Belonoshko AB, Skorodumova NV, Rosengren A, et al. Melting and critical superheating. Phys Rev B 2006;73:012201.
[62] Parrinello M, Rahman A. Crystal-structure and pair potentials – a molecular-dynamics study. Phys Rev Lett 1980;45:1196–9.
[63] Grochala W. Diamond: electronic ground state of carbon at temperatures approaching 0K. Angew Chem Int Ed 2014;53:3680–3.
[64] George J, Reimann C, Deringer VL, et al. On the DFT ground state of crystalline bromine and iodine. Chem Phys Chem 2015;16:728–32.
[65] Yu R, Zhan Q, Zhang X. Elastic stability and electronic structure of pyrite type PtN_2: a hard semiconductor. Appl Phys Lett 2006;88:051913.
[66] Bader RFW. Atoms in molecules: a quantum theory. UK: Clarendon, Oxford; 1990.
[67] Wessel M, Dronskowski R. Nature of N-N bonding within high-pressure noble-metal pernitrides and the prediction of lanthanum pernitride. J Am Chem Soc 2010;132:2421–9.
[68] Peng F, Wang Y, Wang H, et al. Stable xenon nitride at high pressures. Phys Rev B 2015;92:094104.
[69] Li B, Sun H, Chen C. Large indentation strain stiffening in nanotwinned cubic boron nitride. Nat Commun 2014;5:4965.

[70] Roundy D, Krenn CR, Cohen ML, et al. Idear shear strengths of fcc aluminum and copper. Phys Rev Lett 1999;82:2713–6.
[71] Li Q, Sha L, Zhu C, et al. New multifunctional tungsten nitride with energetic N_6 and extreme hardness predicted from first principles. Europhys Lett 2017;118:46001.

Kang Xia is now a Ph.D. candidate studying in Prof. Jian Sun's group at School of Physics, Nanjing University. His current research project focuses on the high-pressure structural design of superhard and high-energy-density materials.

Jian Sun got his B.S. and Ph.D. degree from Nanjing University in 2002 and 2007, respectively. From 2007 to 2013, he worked as a postdoctoral research fellow at NRC Canada, Ruhr University Bochum in Germany and Cavendish Laboratory in University of Cambridge. Since 2013, he has been a professor in School of Physics, Nanjing University. His research interest includes high pressure physics, computational condensed mater physics and materials design.

Hui-Tian Wang is currently a professor in School of Physics, Nanjing University. His research interest covers nonlinear optics, optical field manipulation and condensed mater physics.